A neural system for encoding odor valence which influences approach behaviors

Marie A. Gadziola[1,2,3,#], Lucas A. Stetzik[1,2#], Adrianna J. Milton[3], Keiko Arakawa[3], Daniel W. Wesson[1,2,3,*]

[1]Department of Pharmacology & Therapeutics
[2]Center for Smell & Taste
University of Florida
1200 Newell Dr.
Gainesville, FL, 32610. U.S.A.

[3]Department of Neurosciences
Case Western Reserve University
2109 Adelbert Rd.
Cleveland, OH, 44106. U.S.A.

[#]Equal contributing first-authors

[*]corresponding author: danielwesson@ufl.edu (D.W.)

Running head: Valence and approach in olfaction.

Abstract

Odors may elicit strong emotional and behavioral responses which are known to be strengthened through learning. Presumably subserving this, olfactory structures are well-known for their experience-dependent plasticity, yet the specific cellular systems involved and the actual influence of these systems on behavior are less understood. Here we investigated the transformation of odor information throughout the association of odors with learned-rewarded outcomes and also sought to link those neural systems with displays of reinforcement-based approach behaviors. First, we investigated the representation of odor-reward associations, also known as valence, within two areas recipient of dense olfactory bulb input, the posterior piriform cortex (pPCX) and olfactory tubercle (OT), using simultaneous multi-site electrophysiological recordings from mice engaged in a reward-based olfactory learning task. As expected, neurons in both regions represented the reward-associated valence of odors, yet both the proportion of neurons recruited by conditioned rewarded odors and the magnitudes of their recruitment were distinctly pronounced in the OT. Using fiber photometry we found that odor valence coding in the OT occurs among D1- but not D2-type dopamine receptor expressing neurons. In both the recordings and imaging, statistically meaningful changes in activity occurred prior to instrumental behavior responses. Finally, using optogenetics we show that OT D1-receptor expressing neurons strongly influence reward-motivated approach behavior. Together our results contribute to a model whereby OT D1 neurons support olfactory valence and ultimately hedonic-based behavioral responses.

Key Words

hedonics, motivation, ventral striatum, olfaction, learning

Introduction

Upon learning, stimuli may acquire meaning, also known as valence, which is considered integral in guiding behavioral choice (Berridge and Aldridge, 2008; Chikazoe et al., 2014; Gottfried, 2009; Kumar et al., 2012; Pessoa and Adolphs, 2010; Veldhuizen et al., 2009). Learning to associate a stimulus with an outcome shapes our actions in profound manners – including impacting the choices of foods we eat and can lead to maladaptive outcomes such as those resulting from engaging in compulsive behaviors. This process enables stimuli to hold 'valence' (Lewin, 1935) which is of essence in the execution of behaviors which support satiation of basic needs (Lewin, 1935; Tolman, 1932). Despite holding fundamental importance for our day-to-day actions, the neural systems underlying the generation of valence within the brain are unresolved.

Neural signatures of valence can be observed in the form of flexible expressions of neural activity in response to stimuli throughout reward- or emotion-based associative learning (*e.g.,* (Berridge, 2019; Gore et al., 2015; Hickey and Peelen, 2015; Isosaka et al., 2015; Morrison and Salzman, 2009; Schoenbaum et al., 1998)). This has been well-established in the orbitofrontal cortex and basolateral amygdala, for instance, wherein neurons in these associative structures display differential firing following reinforcement learning for stimuli conditioned to predict a salient outcome (Roesch et al., 2007; Schoenbaum and Eichenbaum, 1995; Schoenbaum et al., 2003).

Behavioral displays linked to the valence of odors have been observed in all animals studied to date and involve a variety of brain systems (Knaden and Hansson, 2014; Li and Liberles, 2015). Olfactory system structures display forms of plasticity (Barnes et al., 2008; Chapuis and Wilson, 2011; Dias and Ressler, 2014; Doucette et al., 2011; Kass et al., 2013; Lebel et al., 2001; Li et al., 2008; Mandairon and Linster, 2009; Murata et al., 2015; Ross and Fletcher, 2018; Schoenbaum et al., 2000), yet in many of these cases the specific cellular systems involved and/or whether those systems specifically influence behavior are less understood. Among these, olfactory cortical structures including both the piriform cortex (PCX) and olfactory tubercle (OT) encode the valence of odors. Specifically, work from several groups including ours (Gadziola et al., 2015; Gire et al., 2013; Roesch et al., 2007; Schoenbaum and Eichenbaum, 1995), have demonstrated that PCX and OT neurons are more greatly recruited by odors conditioned to predict rewards versus those which are unreinforced. These results have indicated that olfactory cortices encode learned odor valence by a combination of recruiting neurons into an ensemble and also divergent firing for rewarded odors.

The representation of odor valence by both PCX and OT neurons leads to the assumption that valence is a distributed, global property of the olfactory cortex. Indeed, that both PCX and OT neurons encode odor valence with divergent firing (Gadziola et al., 2015; Gire et al., 2013;

118 Roesch et al., 2007; Schoenbaum and Eichenbaum, 1995) suggests a possible substrate wherein
119 information within these systems is more-or-less equally relayed into downstream structures
120 important for learning and memory (PCX; (Gottfried, 2010; Wilson and Sullivan, 2011)) or those
121 integral for motivated and affective behaviors (OT; (Wesson and Wilson, 2011; Zhang et al.,
122 2017a)). However, this assumption is not warranted since presently no information exists
123 regarding whether either of these structures are more specialized in their capacity to encode odor
124 valence. As a specific void, no investigations of these structures simultaneously during valence
125 learning exist. Thus, an alternative system may be in place: that olfactory cortices differentially
126 represent odor valence in manners suggesting that one structure is specialized in valence
127 assignment functions. Determining whether valence is a global property distributed among the
128 PCX and OT is an important question in the overall goal of resolving the neural circuitry underlying
129 olfactory valence.

130 Based upon the representation of learned odor valence in the OT (Gadziola et al., 2015;
131 Murata et al., 2015), and the positioning of the OT within the ventral striatum (Heimer et al., 1982;
132 De Olmos and Heimer, 1999) wherein it receives dense innervation from dopaminergic neurons
133 in the ventral tegmental area (Ikemoto, 2007; Voorn et al., 1986), we predicted that the OT is a
134 central figure in assigning odors with valence. Infusion of psychoactive substances into the OT is
135 reinforcing, and rodents more robustly seek infusions into the OT than even into the nucleus
136 accumbens (Ikemoto, 2003) – highlighting the likely importance of OT dopamine in guiding
137 approach behavior, as also indicated by a recent optogenetic study (Zhang et al., 2017b). An
138 additional feature of the OT which supports this hypothesis is its cellular composition. The OT is
139 primarily composed of medium spiny neurons expressing either the D1- or D2-type dopamine
140 receptor (Murata et al., 2015). D1 MSNs in many striatal structures are activated by appetitive
141 stimuli and are often considered integral for promoting stimulus reward and approach, whereas
142 at least some reports indicate D2-type MSNs are less shaped by reinforcement (for reviews (Lobo
143 and Nestler, 2011; Soares-Cunha et al., 2016). Therefore, it is possible that previous reports of
144 neuromodulation driving reinforcement through the OT (Ikemoto, 2003) is due to direct actions
145 upon OT D1-receptor expressing neurons. Supporting this hypothesis, c-Fos expression is
146 elevated in OT D1-type neurons following associative learning (Murata et al., 2015). Based upon
147 the above, we predicted that OT D1-receptor expressing neurons may underlie odor valence
148 representations in the OT and separately, should therefore also be capable of promoting
149 reinforcer-motivated approach behaviors, similar to that needed to subserve engagement with
150 odors.

151 Here we tested the above hypotheses through a combination of multi-site single-unit
152 recordings, cell type-specific fiber photometry, and cell type-specific optogenetic studies, all in
153 mice engaged in reinforcer-motivated operant tasks. All together our results contribute to a model
154 whereby the OT, and specifically OT D1-receptor expressing neurons support olfactory hedonics
155 and ultimately hedonic-based behavioral responses.
156

157 **Results**

158 *Compared to pPCX, neurons in the OT robustly encode valence.*

159 We began by examining whether valence is a global property distributed among the pPCX
160 and OT. We simultaneously monitored OT and posterior PCX (pPCX) single-unit activity from 11
161 mice implanted with chronic electrode arrays (**Fig 1 & S1A**) while they engaged in a head-fixed
162 odor discrimination task requiring them to lick a spout for a palatable reinforcer available at the
163 offset of conditioned-rewarded but not unrewarded odors (**Fig 1B&C**). This head-fixed paradigm
164 allows odor-guided behaviors while maintaining precision in odor-delivery (Verhagen et al., 2007).
165 To optimize the data contributed from each animal, all mice were shaped to discriminate between
166 2-4 odor pairs (Methods). Further, by excluding trials wherein animals prematurely licked during
167 the odor we can reduce influences of motor planning or execution on the neural analyses.
168 Baseline and odor-evoked activity were measured for isolated single neurons. The baseline firing
169 rates of OT (median rate: 3.1 Hz; range = 0 - 56.9 Hz) and pPCX neurons (median rate: 2.1 Hz;
170 range = 0 - 35.6 Hz) were low across the sampled population (**Fig S1B**, measured 2s prior to odor
171 onset). In both structures, odor-evoked firing was observed in response to the odors and occurred
172 soon after odor onset (0.35 ± 0.31s [OT], 0.57 ± 0.48s [pPCX], **Fig 1D**).
173 After mice learned to discriminate between odor pairs (**Fig S1C**) we observed that the
174 majority of OT neurons were significantly modulated in their firing during the task window (65%,
175 52/80 OT neurons 'task-responsive' within 7s of odor onset). This was comparable to the
176 population of pPCX neurons modulated in the same time (X^2(df=1, n=87) = 3.32, p>0.05; 44%,
177 35/79 neurons). To characterize responses across these populations, we measured the temporal
178 response profile of each neuron-odor pair during correct trials by quantifying changes in firing rate
179 from baseline using a sliding receiver operating characteristic (ROC) analysis (Cohen et al., 2012;
180 Gadziola et al., 2015; Veit and Nieder, 2013). Area under the ROC curve (auROC) values greater
181 than 0.5 indicate increases (excitation) in firing rate compared to baseline, with values under 0.5
182 indicating decreases (suppression). This analysis revealed that 91% (189/208) of OT neuron-odor

183 pairs and 78% (110/140) of pPCX neuron-odor pairs displayed significant stimulus-evoked activity
184 during odor presentation, with significant changes in firing rate observed shortly (<500 ms) after
185 odor onset. Of these responses, 71% of OT and 59% of pPCX neurons increased their firing rate
186 relative to baseline, with the remaining neurons suppressing their firing rates relative to baseline.
187 Across the population of neurons from both regions, we observed that OT neurons
188 displayed more divergent responses to the conditioned odors than pPCX neurons, with more
189 robust and longer-lasting responses to conditioned rewarded than unrewarded odors (**Fig 2**). To
190 test whether the populations of OT and pPCX neurons preferentially encode one conditioned odor
191 over the other, we averaged the auROC values computed across the first 500-ms following odor
192 onset. OT neurons preferentially responded to rewarded odor with higher firing than the
193 unrewarded odors (0.59 ± 0.02 vs 0.55 ± 0.01, respectively; paired *t* test: $t_{(103)} = -6.05$, $p <$
194 0.0001), whereas pPCX neurons did not respond differentially to rewarded and unrewarded odors
195 across the population (0.53 ± 0.01 vs 0.53 ± 0.01, respectively; paired *t* test: $t_{(69)} = -0.73$, $p =$
196 0.47). Furthermore, average auROC values in response to rewarded odors were greater for the
197 population of OT neurons when compared to pPCX neurons (0.59 ± 0.02 vs 0.53 ± 0.01,
198 respectively; two-sample *t* test: $t_{(172)} = -3.49$, $p < 0.001$). There were no discernable differences in
199 the temporal response pattern of neurons that increased vs decreased firing rates, suggesting
200 that these neurons are similarly driven by conditioned odors (**Fig S2**). Next, we compared the
201 duration of significant auROC responses in the first 500ms after odor onset across the population
202 of neurons in both regions (including units with ≥ 1 significant bin). OT responses were
203 significantly longer in duration compared to pPCX responses (209 ± 97 vs 166 ± 91 ms,
204 respectively; two-sample *t* test: $t_{(290)} = -3.64$, $p < 0.001$). In addition, OT response durations to
205 rewarded odors were longer than unrewarded odors (225 ± 94 vs 193 ± 98 ms, respectively;
206 paired *t* test: $t_{(96)} = -12.01$, $p < 0.0001$), and longer than pPCX responses to rewarded odors (225
207 ± 94 vs 167 ± 84 ms, respectively; two-sample *t* test: $t_{(141)} = -3.51$, $p < 0.0001$). These results
208 support the conclusion that the representation of odor valence is not equally distributed among
209 the OT and pPCX – with the OT dominating in assigning valence.
210

211 *D1 receptor expressing OT neurons display divergent responses to conditioned rewarded odors.*

212 Which neurons are responsible for the pronounced display of valence in the OT? We
213 addressed this question by performing fiber photometry-based imaging (*e.g.,* (Gunaydin et al.,
214 2014; Kudo et al., 1992)) of GCaMP6f (Chen et al., 2013) from D1 and D2 receptor-expressing

215 neurons in the OT. Mice expressing Cre-recombinase in either neurons expressing the D1
216 receptor (D1-Cre) or D2 receptor (D2-Cre) (Gong et al., 2003) were injected with floxed GCaMP6f
217 into their OT and later implanted with optical fibers (see Methods) before being water deprived
218 and shaped in the same lick/no-lick odor discrimination task used above. During imaging (**Figs**
219 **3A-C**), the GCaMP6f emission spectrum was collected as a measure of aggregate OT D1 or D2
220 neuron activity. Simultaneously, from all recordings, we also collected endogenous UV emission
221 spectrum as a control measure for movement artifacts. The resultant GCaMP6f signal was
222 subtracted from the UV signal for a single output, which is considered closely reflective of
223 aggregate neural activity. In separate experiments we confirmed that GCaMP6f expression
224 robustly colocalizes with D1 and D2 receptor expressing neurons in these Cre lines by crossing
225 the Ai9 TdTomato reporter line (Madisen et al., 2012) with the D1-Cre and D2-Cre mice. The
226 resultant D1-Cre;Ai9 and D2-Cre;Ai9 mice were injected with floxed GCaMP6f into their OT and
227 allowed to recover 2 weeks prior to tissue collection. High levels of colocalization were found in
228 the OTs of both lines (**Fig 3A**; D1-Cre;Ai9: 95.01 ± 0.96 [inter-animal range 94.0-95.9]; D2-
229 Cre;Ai9: 95.52 ± 1.7 [inter-animal range 93.6-97.0] mean ± sd), thus confirming the targeted
230 specificity of GCaMP to the desired cell populations.

231 We imaged 5 D1- and 5 D2-Cre mice with fiber implants and GCaMP6f expression both
232 confirmed in the OT (**Fig S3**) throughout learning and performance in the lick/no-lick odor
233 discrimination task. To enhance each animal's contributions for a more rigorous data set, we
234 shaped each mouse on several odor pairs over differing daily sessions, yet only one pair of odors
235 in a given session. This allowed each animal to contribute odor-modulated GCaMP6f signals to
236 2-3 rewarded and unrewarded odors (on different sessions) at or above criterion performance
237 (mean rewarded odor trials / session = 44.5 [24-75 min-max range]; mean unrewarded odor trials
238 / session = 91.3 [52-133 min-max range]). Across all rewarded and unrewarded odors, we
239 observed modulations in both D1 and D2 neuron activity following odor onset. This was evident
240 both looking within individual mice at subsets of trials (**Fig 3C & D**), and averaged across mice
241 over several sessions (**Fig 3E & F**). No discernable differences were observed in the time prior
242 to odor onset, or before 0.5s following odor onset between any stimulus type in either D1 or D2
243 mice (**Fig 3E & F**). Later during the odor period however (0.5-0.75s), across all D1 mice,
244 conditioned rewarded and unrewarded odors elicited differing amounts of activity (p<0.001; **Fig**
245 **3E**). Whereas D1 neurons were largely unmodulated by the conditioned unrewarded odor,
246 conditioned rewarded odors elicited large increases in activity during the odor. In contrast, no
247 differential representation of conditioned rewarded versus unrewarded odors was observed in D2

248 mice, with both conditioned stimuli eliciting similar increases in activity during odor (*p*=0.483; **Fig**
249 **3F**).

250

251 *The responses of D1 receptor-expressing OT neurons are flexible and encode the associated*
252 *outcomes of odors.*

253 Having imaged D1 and D2-type receptor expressing OT neurons and observing that they
254 differently encode odor-reward associations, we were next able to ask whether this differential
255 representation of conditioned rewarded odors observed among the D1 neuron population is
256 flexible. In other words, does the representation of conditioned-rewarded odors flexibly follow as
257 odors are associated to predict new outcomes? To address this, in a separate behavioral session
258 we used reversal learning to reverse the odor-outcome contingencies so that a previously
259 rewarded odor is no longer rewarded and a previously unrewarded odor is now rewarded. Most
260 mice were shaped upon at least 2 odor-reversals (differing odor pairs, range 2-3). If a population
261 of neurons is 'identity' encoding they should exhibit the same odor selectivity before and after
262 reversal learning, whereas a population encoding the associative valence of an odor (rewarded
263 or not) should reverse its odor preference (Gire et al., 2013; Roesch et al., 2007). Animals took
264 several sessions to learn the reversal to criterion in this task requiring them to withhold licking
265 until odor offset, and comparisons were made only from sessions following task acquisition, during
266 blocks consisting of criterion-level performance, and correct responses during each trial.

267 On average across animals, the evoked GCaMP6f signals in D1-Cre mice tracked the
268 behavioral contingencies – with the original rewarded odor and the newly rewarded odor eliciting
269 evoked responses with similar amplitudes (*p*=0.202; **Fig. 3G**). Likewise, the original unrewarded
270 odors elicited similar responses as the new unrewarded odors (*p*=0.177). In contrast, no effect of
271 reversal on either the rewarded (*p*=0.785) or unrewarded odors (*p*=0.522) were observed in the
272 D2-Cre mice (**Fig. 3H**). D2 neurons maintained somewhat positive responses for all odors,
273 regardless of valence, indicating that while these neurons are modulated by odor, they do not
274 represent odor valence. These data support our hypothesis that specifically D1 receptor-
275 expressing neurons are responsible for the profound representation of odor valence in the OT.

276

277 *OT D1 receptor-expressing neurons drive robust approach behaviors.*

278 Having observed reward-associated odor valence coding in OT D1, but not D2 receptor-
279 expressing neurons, we next asked whether the activity of these neurons directly influences the
280 occurrence of approach behaviors. Indeed, the latency and robustness of OT D1 neuron encoding
281 of conditioned rewarded odors may serve as an effective way whereby to activate approach
282 behaviors. To test this, D1-Cre mice injected with a floxed AAV encoding channelrhodopsin
283 (ChR2) [n = 7] (or floxed AAV encoding a reporter fluorophore [n = 5]) into their ventral striatum
284 were later implanted with an unilateral optical fiber into their OT (**Fig 4A**). Mice were shaped in
285 an optical intra-cranial self-stimulation task, adapted from (Carlezon and Chartoff, 2007; Ilango et
286 al., 2014; Vicente et al., 2016), allowing for assaying of stimulation-seeking goal-directed
287 behaviors (**Fig 4B**). Shaping in this instrumental task occurred over several phases (See
288 Methods). In the first phase, mice could poke their snout into either of two ports in exchange for
289 blue light stimulation into their OT (25Hz, for 2s, fixed ratio 1). All but one of the D1-Cre mice
290 injected with AAV.ChR2 reached a set level of criterion performance (40 pokes into either port
291 during a 1 hr session)(**Fig 4C**), indicating that they readily learned to poke in exchange for blue
292 light stimulation. No control AAV injected mice reached criterion performance (**Fig 4C**). The mice
293 reaching criterion on Phase 1 then progressed onto Phase 2 wherein only one of the two ports
294 delivered light. The port receiving the greater number of pokes during Phase 1 was selected as
295 the 'active' port for Phase 2. The vast majority of AAV.ChR2 mice (5/6) reached criterion on Phase
296 2, with some poking over 500 times in the single hour of testing (**Fig 4Di & ii**). To ensure that
297 these mice were indeed seeking light stimulation, on the subsequent Phase 3, the location of the
298 active port was reversed and despite this, all the mice who reached criterion on Phase 2 redirected
299 their responding to criterion levels for the new active port. Compared to the first session of reversal
300 phase testing, there were significantly more pokes for the active port during both the last session
301 of phase 2 testing (p=0.0002), as well as during the last session of reversal (p=0.0004). These
302 results indicate that OT neurons expressing the D1-type dopamine receptor support behavioral
303 approach, specifically by signaling reinforcement.

304

305 **Discussion**

306 The olfactory system holds a remarkable capacity for experience-based plasticity and informing
307 a wide-range of critical behaviors. Olfactory structures, including those more associative in nature
308 (*e.g.,* the orbitofrontal cortex), are well-known for their plasticity (Barnes et al., 2008; Chapuis and
309 Wilson, 2011; Dias and Ressler, 2014; Doucette et al., 2011; Kass et al., 2013; Lebel et al., 2001;

310 Li et al., 2008; Mandairon and Linster, 2009; Murata et al., 2015; Ross and Fletcher, 2018;
311 Schoenbaum et al., 2000), yet in many of these cases the specific cellular systems involved and/or
312 whether those systems specifically influence behavior is less understood. Here we build off of
313 previous studies which have uncovered odor-reward association-based plasticity among neurons
314 in both the PCX and OT (in separate studies; (Calu et al., 2007; Gadziola et al., 2015; Gire et al.,
315 2013)) to interrogate the respective roles of each of these structures in the representation of odor
316 valence by means of simultaneous single-unit recordings. After identifying robust odor valence
317 coding among neurons in the OT significantly more-so than those in the pPCX, we employed fiber
318 photometry in D1-Cre and D2-Cre mice to uncover evidence indicating that OT D1-, but not D2-
319 type dopamine receptor expressing neurons encode odor valence. Finally, we linked the activity
320 of OT D1 neurons to the display of reward-driven behaviors, specifically approach behaviors.

321 This work adds to a growing body of literature seeking to understand the brain systems
322 governing the generation of stimulus hedonics and preferences (for review (Berridge and
323 Kringelbach, 2015)). Attraction to odors is well established and may employ innate (unlearned) or
324 acquired (learned) mechanisms. Since the olfactory bulb is the starting-point for odor perception,
325 it is not surprising that the olfactory bulb holds importance for both innate and learned odor
326 hedonics (*e.g.,* (Doucette et al., 2011; Kermen et al., 2016; Kobayakawa et al., 2007; Wilson et
327 al., 1987). Indeed, recent work uncovered evidence that a specific zone within the main olfactory
328 bulb is necessary for generating odor hedonics (Kermen et al., 2016). The hedonic information of
329 odors in the OB next may be distributed into the OT and PCX. Both PCX and OT neurons may
330 be recruited to encode odor valence and do so with divergent firing to conditioned rewarded
331 versus unrewarded odors (Gadziola et al., 2015; Gire et al., 2013; Roesch et al., 2007;
332 Schoenbaum and Eichenbaum, 1995). A key prediction in this work was that OT units would more
333 greatly represent odor valence than those in the PCX. That said, it is quite surprising the
334 magnitude at which we found this occurs. OT units far surpassed the size of the population of
335 pPCX units encoding valence and also exceeded pPCX units in their magnitude of firing for
336 conditioned rewarded odors. This inter-regional difference could not simply be the result of
337 behavioral, affective, or other state-dependent influences since recordings were sampled from
338 both the pPCX and OT simultaneously. Thus, this work uncovers that systems downstream from
339 the OB are specialized in their representation of odor valence. This outcome is consistent with
340 our hypothesis and also that of other groups (Kermen et al., 2016; Murata et al., 2015).

341 Specific cell populations in several brain regions have been linked to stimulus valence or
342 to approach responses (Betley et al., 2015; Kim et al., 2019; Li and Liberles, 2015; Li et al., 2019;
343 Miller et al., 2019; Soares-Cunha et al., 2016). This work adds OT D1 receptor expressing
344 neurons, in an underappreciated ventral striatum structure, the OT, to this list and suggests a
345 model wherein OT D1-MSNs may signal to downstream systems which also influence approach
346 like the amygdala or hypothalamic nuclei. This model, as also supported by immediate early gene
347 mapping experiments following olfactory learning (Murata et al., 2015), would be potentially
348 powerful in cases wherein odors associated with positive outcomes, which as we show here are
349 represented in OT D1 neurons, could influence downstream limbic systems to strengthen
350 approach responding through their coordinated output.

351 All together these results support a role for OT D1 neurons, not unlike D1 neurons in the
352 nucleus accumbens (Lobo and Nestler, 2011), in behaviors integral for valence -- reinforcement
353 and stimulus-seeking. To come to this conclusion, we used a straight-forward instrumental
354 responding paradigm wherein mice were allowed to nose-poke in exchange for OT D1 neuron
355 stimulation. This paradigm has several advantages over real-time place preference testing or
356 other tests which serve to assay approach behaviors since it allows for measures of discrete,
357 stimulus (*i.e.*, light) seeking behaviors (nose-pokes). The finding that some animals responded at
358 the rate they did, indeed up to 500 pokes in an hour, provides a compelling demonstration that
359 these neurons influence motivation states, or tap into reward circuitry, in a manner which
360 promotes approach behavior. This test was done in the absence of any experimentally-delivered
361 odors which further reinforces the notion that optical stimulation of OT D1 neurons engages
362 important internal circuitry for guiding behavior, versus that which may get paired with odor
363 information entering the OT from the olfactory bulb. OT D1 MSNs send efferents throughout the
364 brain's affective and sensory centers (Zhang et al., 2017a). What specific output targets of OT D1
365 cells are responsible for approach responses will be an important question for future research to
366 address.

367 Taken together, our results contribute to a model whereby the OT is a specialized center
368 for encoding odor valence. This along with the finding that OT D1 neurons encode olfactory
369 valence and robustly motivate reinforcement-seeking in a nose-poke based task which emulates
370 snout-directed investigation behaviors like those used by rodents to sample odors, leads us to
371 predict that OT D1-type MSNs are a fundamental component of brain systems needed to inform
372 and respond to the hedonics of odors.

Acknowledgements: This work was supported by NIH NIDCD grants R01DC014443 and R01DC016519 to D.W. Some mouse strains used in this research were obtained from the Mutant Mouse Regional Resource Center (MMRRC), an NIH funded strain repository, and were donated to the MMRRC by the MMRRC facility at the University of California, Davis.

Author Contributions: Conceptualization: M.A.G., L.A.S., D.W.W.; Methodology: M.A.G., L.A.S., D.W.W.; Investigation: M.A.G., L.A.S., A.J.M., K.A., D.W.W.; Writing – Original Draft: M.A.G., L.A.S., D.W.W.; Writing – Review & Editing: M.A.G., L.A.S., D.W.W.; Visualization: M.A.G., L.A.S., D.W.W.; Supervision: D.W.W.; Funding Acquisition: D.W.W.

Declaration of Interests: The authors declare no competing interests.

399 **References**

400 Barnes, D.C., Hofacer, R.D., Zaman, A.R., Rennaker, R.L., and Wilson, D.A. (2008). Olfactory
401 perceptual stability and discrimination. Nat Neurosci *11*, 1378–1380.

402 Berridge, K.C. (2019). Affective valence in the brain: modules or modes? Nat. Rev. Neurosci.
403 *20*, 225–234.

404 Berridge, K.C., and Aldridge, J.W. (2008). Decision utility, the brain, and pursuit of hedonic
405 goals. Soc. Cogn. *26*, 621–646.

406 Berridge, K.C., and Kringelbach, M.L. (2015). Pleasure systems in the brain. Neuron *86*, 646–
407 664.

408 Betley, J.N., Xu, S., Cao, Z.F.H., Gong, R., Magnus, C.J., Yu, Y., and Sternson, S.M. (2015).
409 Neurons for hunger and thirst transmit a negative-valence teaching signal. Nature *521*, 180.

410 Calu, D.J., Roesch, M.R., Stalnaker, T.A., and Schoenbaum, G. (2007). Associative Encoding in
411 Posterior Piriform Cortex during Odor Discrimination and Reversal Learning. Cereb Cortex *17*,
412 1342–1349.

413 Carlezon, W.A., and Chartoff, E.H. (2007). Intracranial self-stimulation (ICSS) in rodents to
414 study the neurobiology of motivation. Nat. Protoc. *2*, 2987–2995.

415 Chapuis, J., and Wilson, D.A. (2011). Bidirectional plasticity of cortical pattern recognition and
416 behavioral sensory acuity. Nat Neurosci *15*, 155–161.

417 Chen, T.-W., Wardill, T.J., Sun, Y., Pulver, S.R., Renninger, S.L., Baohan, A., Schreiter, E.R.,
418 Kerr, R.A., Orger, M.B., Jayaraman, V., et al. (2013). Ultrasensitive fluorescent proteins for
419 imaging neuronal activity. Nature *499*, 295–300.

420 Chikazoe, J., Lee, D.H., Kriegeskorte, N., and Anderson, A.K. (2014). Population coding of
421 affect across stimuli, modalities and individuals. Nat Neurosci *17*, 1114–1122.

422 Cohen, J.Y., Haesler, S., Vong, L., Lowell, B.B., and Uchida, N. (2012). Neuron-type-specific
423 signals for reward and punishment in the ventral tegmental area. Nature *482*, 85–88.

424 Dias, B.G., and Ressler, K.J. (2014). Parental olfactory experience influences behavior and
425 neural structure in subsequent generations. Nat Neurosci *17*, 89–96.

426 Doucette, W., Gire, D.H., Whitesell, J., Carmean, V., Lucero, M.T., and Restrepo, D. (2011).
427 Associative Cortex Features in the First Olfactory Brain Relay Station. Neuron *69*, 1176–1187.

428 Gadziola, M.A., and Wesson, D.W. (2016). The Neural Representation of Goal-Directed Actions
429 and Outcomes in the Ventral Striatum's Olfactory Tubercle. J. Neurosci. *36*, 548–560.

430 Gadziola, M.A., Tylicki, K.A., Christian, D.L., and Wesson, D.W. (2015). The Olfactory Tubercle
431 Encodes Odor Valence in Behaving Mice. J. Neurosci. *35*, 4515–4527.

432 Gire, D.H., Whitesell, J.D., Doucette, W., and Restrepo, D. (2013). Information for decision-
433 making and stimulus identification is multiplexed in sensory cortex. Nat Neurosci *16*, 991–993.

434 Gong, S., Zheng, C., Doughty, M.L., Losos, K., Didkovsky, N., Schambra, U.B., Nowak, N.J.,
435 Joyner, A., Leblanc, G., Hatten, M.E., et al. (2003). A gene expression atlas of the central
436 nervous system based on bacterial artificial chromosomes. Nature *425*, 917–925.

437 Gore, F., Schwartz, E.C., Brangers, B.C., Aladi, S., Stujenske, J.M., Likhtik, E., Russo, M.J.,
438 Gordon, J.A., Salzman, C.D., and Axel, R. (2015). Neural Representations of Unconditioned
439 Stimuli in Basolateral Amygdala Mediate Innate and Learned Responses. Cell *162*, 134–145.

440 Gottfried, J.A. (2009). Olfaction and Its Pleasures: Human Neuroimaging Perspectives. In
441 Pleasures of the Brain, M.L. Kringelbach, and K.C. Berridge, eds. (Oxford University Press), pp.
442 125–145.

443 Gottfried, J.A. (2010). Central mechanisms of odour object perception. Nat Rev Neurosci *11*,
444 628–641.

445 Green, D.M., and Swets, J.A. (1966). Signal detection theory and psychophysics (New York:
446 Wiley).

447 Gunaydin, L.A., Grosenick, L., Finkelstein, J.C., Kauvar, I. V., Fenno, L.E., Adhikari, A.,
448 Lammel, S., Mirzabekov, J.J., Airan, R.D., Zalocusky, K.A., et al. (2014). Natural Neural
449 Projection Dynamics Underlying Social Behavior. Cell *157*, 1535–1551.

450 Heimer, L., Switzer, R.D., and Van Hoesen, G.W. (1982). Ventral striatum and ventral pallidum:
451 Components of the motor system? Trends Neurosci. *5*, 83–87.

452 Hickey, C., and Peelen, M.V. (2015). Neural Mechanisms of Incentive Salience in Naturalistic
453 Human Vision. Neuron *85*, 512–518.

454 Ikemoto, S. (2003). Involvement of the Olfactory Tubercle in Cocaine Reward: Intracranial Self-
455 Administration Studies. J. Neurosci. *23*, 9305–9311.

456 Ikemoto, S. (2007). Dopamine reward circuitry: Two projection systems from the ventral
457 midbrain to the nucleus accumbens-olfactory tubercle complex. Brain Res Rev *56*, 27–78.

458 Ilango, A., Kesner, A.J., Keller, K.L., Stuber, G.D., Bonci, A., and Ikemoto, S. (2014). Similar
459 Roles of Substantia Nigra and Ventral Tegmental Dopamine Neurons in Reward and Aversion.
460 J. Neurosci. *34*, 817–822.

461 Isosaka, T., Matsuo, T., Yamaguchi, T., Funabiki, K., Nakanishi, S., Kobayakawa, R., and
462 Kobayakawa, K. (2015). Htr2a-Expressing Cells in the Central Amygdala Control the Hierarchy
463 between Innate and Learned Fear. Cell *163*, 1153–1164.

464 Kass, M.D., Rosenthal, M.C., Pottackal, J., and McGann, J.P. (2013). Fear Learning Enhances
465 Neural Responses to Threat-Predictive Sensory Stimuli. Science (80-.). *342*, 1389–1392.

466 Kermen, F., Midroit, M., Kuczewski, N., Forest, J., Thevenet, M., Sacquet, J., Benetollo, C.,
467 Richard, M., Didier, A., and Mandairon, N. (2016). Topographical representation of odor
468 hedonics in the olfactory bulb. Nat Neurosci *19*, 876–878.

469 Kim, J., Lee, S., Fang, Y.-Y., Shin, A., Park, S., Hashikawa, K., Bhat, S., Kim, D., Sohn, J.-W.,
470 Lin, D., et al. (2019). Rapid, biphasic CRF neuronal responses encode positive and negative
471 valence. Nat. Neurosci. *22*, 576–585.

472 Knaden, M., and Hansson, B.S. (2014). Mapping odor valence in the brain of flies and mice.
473 Curr. Opin. Neurobiol. *24*, 34–38.

474 Kobayakawa, K., Kobayakawa, R., Matsumoto, H., Oka, Y., Imai, T., Ikawa, M., Okabe, M.,
475 Ikeda, T., Itohara, S., Kikusui, T., et al. (2007). Innate versus learned odour processing in the
476 mouse olfactory bulb. Nature *450*, 503–508.

477 Kudo, Y., Akita, K., Nakamura, T., Ogura, A., Makino, T., Tamagawa, A., Ozaki, K., and
478 Miyakawa, A. (1992). A single optical fiber fluorometric device for measurement of intracellular
479 Ca2+ concentration: Its application to hippocampal neurons in vitro and in vivo. Neuroscience
480 *50*, 619–625.

481 Kumar, S., von Kriegstein, K., Friston, K., and Griffiths, T.D. (2012). Features versus Feelings:

482 Dissociable Representations of the Acoustic Features and Valence of Aversive Sounds. J.
483 Neurosci. *32*, 14184–14192.

484 Lebel, D., Grossman, Y., and Barkai, E. (2001). Olfactory learning modifies predisposition for
485 long-term potentiation and long-term depression induction in the rat piriform (olfactory) cortex.
486 Cereb. Cortex *11*, 485–489.

487 Lewin, K. (1935). A Dynamic Theory of Personality (McGraw-Hill Book Company, Inc.).

488 Li, Q., and Liberles, S.D. (2015). Aversion and attraction through olfaction. Curr. Biol. *25*, R120–
489 R129.

490 Li, H., Pullmann, D., Cho, J.Y., Eid, M., and Jhou, T.C. (2019). Generality and opponency of
491 rostromedial tegmental (RMTg) roles in valence processing. Elife *8*, e41542.

492 Li, W., Howard, J.D., Parrish, T.B., and Gottfried, J.A. (2008). Aversive learning enhances
493 perceptual and cortical discrimination of indiscriminable odor cues. Science (80-.). *319*, 1842–
494 1845.

495 Lobo, M.K., and Nestler, E.J. (2011). The Striatal Balancing Act in Drug Addiction: Distinct
496 Roles of Direct and Indirect Pathway Medium Spiny Neurons. Front. Neuroanat. *5*, 41.

497 Madisen, L., Mao, T., Koch, H., Zhuo, J., Berenyi, A., Fujisawa, S., Hsu, Y.-W.A., Garcia, A.J.,
498 Gu, X., Zanella, S., et al. (2012). A toolbox of Cre-dependent optogenetic transgenic mice for
499 light-induced activation and silencing. Nat Neurosci *15*, 793–802.

500 Mandairon, N., and Linster, C. (2009). Odor perception and olfactory bulb plasticity in adult
501 mammals. J. Neurophysiol. *101*, 2204–2209.

502 Miller, S.M., Marcotulli, D., Shen, A., and Zweifel, L.S. (2019). Divergent medial amygdala
503 projections regulate approach–avoidance conflict behavior. Nat. Neurosci. *22*, 565–575.

504 Morrison, S.E., and Salzman, C.D. (2009). The Convergence of Information about Rewarding
505 and Aversive Stimuli in Single Neurons. J. Neurosci. *29*, 11471–11483.

506 Murata, K., Kanno, M., Ieki, N., Mori, K., and Yamaguchi, M. (2015). Mapping of Learned Odor-
507 Induced Motivated Behaviors in the Mouse Olfactory Tubercle. J. Neurosci. *35*, 10581–10599.

508 De Olmos, J.S., and Heimer, L. (1999). The Concepts of the Ventral Striatopallidal System and

509 Extended Amygdala. Ann. N. Y. Acad. Sci. *877*, 1–32.

510 Paxinos, G., and Franklin, K. (2000). The Mouse Brain in Stereotaxic Coordinates (San Diego:
511 Academic Press).

512 Pessoa, L., and Adolphs, R. (2010). Emotion processing and the amygdala: from a “low road” to
513 “many roads” of evaluating biological significance. Nat Rev Neurosci *11*, 773–783.

514 Roesch, M.R., Stalnaker, T.A., and Schoenbaum, G. (2007). Associative encoding in anterior
515 piriform cortex versus orbitofrontal cortex during odor discrimination and reversal learning.
516 Cereb Cortex *17*, 643–652.

517 Ross, J.M., and Fletcher, M.L. (2018). Learning-Dependent and -Independent Enhancement of
518 Mitral/Tufted Cell Glomerular Odor Responses Following Olfactory Fear Conditioning in Awake
519 Mice. J. Neurosci.

520 Schoenbaum, G., and Eichenbaum, H. (1995). Information coding in the rodent prefrontal
521 cortex. I. Single-neuron activity in orbitofrontal cortex compared with that in pyriform cortex. J
522 Neurophysiol *74*, 733–750.

523 Schoenbaum, G., Chiba, A.A., and Gallagher, M. (1998). Orbitofrontal cortex and basolateral
524 amygdala encode expected outcomes during learning. Nat Neurosci *1*, 155–159.

525 Schoenbaum, G., Chiba, A.A., and Gallagher, M. (2000). Changes in functional connectivity in
526 orbitofrontal cortex and basolateral amygdala during learning and reversal training. J Neurosci
527 *20*, 5179–5189.

528 Schoenbaum, G., Setlow, B., Saddoris, M.P., and Gallagher, M. (2003). Encoding predicted
529 outcome and acquired value in orbitofrontal cortex during cue sampling depends upon input
530 from basolateral amygdala. Neuron *39*, 855–867.

531 Soares-Cunha, C., Coimbra, B., Sousa, N., and Rodrigues, A.J. (2016). Reappraising striatal
532 D1- and D2-neurons in reward and aversion. Neurosci. Biobehav. Rev. *68*, 370–386.

533 Thompson, K.G., Hanes, D.P., Bichot, N.P., and Schall, J.D. (1996). Perceptual and motor
534 processing stages identified in the activity of macaque frontal eye field neurons during visual
535 search. J. Neurophysiol. *76*, 4040–4055.

536 Tolman, E. (1932). Purposive Behavior (New York: Appleton-Century).

537 Veit, L., and Nieder, A. (2013). Abstract rule neurons in the endbrain support intelligent
538 behaviour in corvid songbirds. Nat Commun *4*, 2878.

539 Veldhuizen, M.G., Rudenga, K.J., and Small, D.M. (2009). The pleasure of taste, flavor, and
540 food. In Pleasures of the Brain, M.L. Kringelbach, and K.C. Berridge, eds. (Oxford University
541 Press), pp. 146–168.

542 Verhagen, J. V, Wesson, D.W., Netoff, T.I., White, J.A., and Wachowiak, M. (2007). Sniffing
543 controls an adaptive filter of sensory input to the olfactory bulb. Nat Neurosci *10*, 631–639.

544 Vicente, A.M., Galvão-Ferreira, P., Tecuapetla, F., and Costa, R.M. (2016). Direct and indirect
545 dorsolateral striatum pathways reinforce different action strategies. Curr. Biol. *26*, R267–R269.

546 Voorn, P., Jorritsma-Byham, B., Van Dijk, C., and Buijs, R.M. (1986). The dopaminergic
547 innervation of the ventral striatum in the rat: A light- and electron-microscopical study with
548 antibodies against dopamine. J. Comp. Neurol. *251*, 84–99.

549 Wesson, D.W., and Wilson, D.A. (2011). Sniffing out the contributions of the olfactory tubercle to
550 the sense of smell: hedonics, sensory integration, and more? Neurosci Biobehav Rev *35*, 655–
551 668.

552 Wilson, D.A., and Sullivan, R.M. (2011). Cortical processing of odor objects. Neuron *72*, 506–
553 519.

554 Wilson, D.A., Sullivan, R.M., and Leon, M. (1987). Single-unit analysis of postnatal olfactory
555 learning: modified olfactory bulb output response patterns to learned attractive odors. J
556 Neurosci *7*, 3154–3162.

557 Zhang, Z., Zhang, H., Wen, P., Zhu, X., Wang, L., Liu, Q., Wang, J., He, X., Wang, H., and Xu,
558 F. (2017a). Whole-Brain Mapping of the Inputs and Outputs of the Medial Part of the Olfactory
559 Tubercle. Front. Neural Circuits *11*, 52.

560 Zhang, Z., Liu, Q., Wen, P., Zhang, J., Rao, X., Zhou, Z., Zhang, H., He, X., Li, J., Zhou, Z., et
561 al. (2017b). Activation of the dopaminergic pathway from VTA to the medial olfactory tubercle
562 generates odor-preference and reward. Elife *6*.

563

564

565 **Figure Legends**

566 **Figure 1. Paradigm for investigating the distribution of odor valence encoding among**
567 **olfactory cortices. A)** Recording schematic indicating simultaneous monitoring of OT and pPCX
568 activity with multi-channel arrays in mice (8 wires/region). pPCX and OT activity were recorded
569 on opposite hemispheres within mice. **B)** Schematic of head-fixed behavioral set-up and **C)**
570 experimental trial outline. Water-deprived mice implanted with chronic multi-site arrays into their
571 OT and pPCX (as in A) and a head-bar were acclimated to head restraint and shaped in a lick/no-
572 lick odor discrimination task wherein following a variable inter-trial interval (ITI) one odor signaled
573 the availability of a small palatable fluid reward from a reward spout following odor offset (during
574 the 'lick reward available' epoch). Alternative (unreinforced) odors were conditioned to not signal
575 reward availability. OT and pPCX unit activity was acquired throughout performance in the task.
576 **D)** Example OT and pPCX unit activity indicating odor valence encoding by neurons in both
577 structures. Multiunit activity (MUA) was spike sorted off-line to identify single-unit activity (SUA)
578 using template matching and cluster cutting with principal component analyses. Vertical lines on
579 the lick trace indicate timing of individual licks (detected with an infrared photo-beam in front of
580 the lick spout). Vertical scale bar applies to both OT and pPCX MUA channels. Data are from two
581 consecutive trials.

582 **Figure 2. OT neurons display greater divergent responses to conditioned odors than pPCX.**
583 **A**) Time course of odor-evoked changes in firing rate relative to baseline as indicated by auROC
584 in response to unrewarded and rewarded odors in the pPCX (left; n=70 neurons) and OT (right;
585 n=104 neurons). Each row represents one single responsive neuron, and neurons are sorted by
586 baseline rates during rewarded odor trials (top row = lowest rate). **B**) Population average auROC
587 values for all responsive neurons in response to rewarded and unrewarded odors compared
588 against a shuffled control distribution. Both regions show an increase in auROC values >0.5
589 shortly after odor onset, indicating increases in firing relative to baseline. Across the population,
590 OT neurons displayed more divergent responses to conditioned odors than pPCX neurons, with
591 the rewarded odor eliciting larger and more persistent changes to firing rate relative to the
592 unrewarded odor. Population values represent the mean ± SEM.

593 **Figure 3. D1 receptor expressing neurons underlie odor valance coding in the OT. Ai)**
594 Example images of GCaMP6f expression in D1- and D2-Cre mice crossed with the rosa
595 Ai9.TdTomato reporter line which were later injected with GCaMP6f. In both Cre lines, GCaMP6f
596 colocalized robustly with the targeted cells (**Aii**). Data points in Aii = means of individual mice (4-

597 5 sections/mouse). Dashed lines define approximate OT cell layers and its ventral boundary. **B)**
598 Example localization of an optical fiber implant into a mouse injected with GCamP6f (green). The
599 optical fiber was positioned to terminate immediately dorsal to the OT. **C)** Schematic of the fiber
600 photometry system for use in head-fixed behaving mice. 465nm and 405nm LEDs excitation
601 wavelengths passed through dichroic mirrors prior to being sent into the implanted optical fiber
602 via a patch cable. GCaMP6f and UF emission were then both amplified by femtowatt
603 photoreceivers prior to being digitized simultaneously with behavioral data and stimulus
604 presentation events. Please see Fig 1 for a description of the head-fixed paradigm. Example
605 GCaMP6f responses to the original rewarded and unrewarded odors in a single D1-Cre **(D)** and
606 D2-Cre mouse **(E)** averaged over 10 trials of correct behavioral responses during blocks of
607 criterion behavioral performance. These example averaged traces indicate divergent responses
608 to the original rewarded odor vs the original unrewarded odor in D1-Cre but not D2-Cre mice,
609 which is maintained at the population level when averaging across 5 mice, throughout 2-3
610 sessions during criterion behavioral performance (**F & G**). The encoding of odor valence in D1-
611 Cre mice (as in **F**) was confirmed in experiments wherein the odor-reward contingencies were
612 reversed (original rewarded = no unrewarded, and vice versa) (**H & I**). Insets in **H & I** display the
613 mean delta f/f during 0.5-0.75sec of odor in for all four stimulus types. ***=p<0.001. ns = not
614 significant (p>0.05). No significance was found in any planned comparison in the D2-Cre mice (**I**).

615 **Figure 4**. **OT neurons expressing the D1 receptor promote reinforcement and approach**
616 **behaviors. (A)** Optical fiber implant locations from mice contributing optical-intracranial self-
617 stimulation data (opto-ICSS), segregated based upon those mice which learned versus failed to
618 acquire phase 1 of the task. **(B)** Opto-ICSS task schematic wherein mice were required to nose
619 poke in exchange for blue-light mediated optogenetic excitation of OT D1 neurons. At least 2
620 weeks following injection with either a floxed AAV encoding ChR2 and a reporter fluorophore
621 (AAV.ChR2) or a floxed AAV solely encoding a reporter fluorophore (AAV), mice were shaped on
622 the opto-ICSS task. Please see text for a description of the four task phases. **(C)** Pie chart
623 indicating that all but one AAV.ChR2 mouse reached criterion performance on phase 1 of the
624 task. **(Di)** Performance of two example mice during phases 2-4 of the opto-ICSS task. The mice
625 displayed diversity in their number of pokes into the active port, and in their % of pokes displayed
626 for the active (blue-light emitting) versus inactive ports. Both of these mice reached criterion on
627 phase 2 and phase 3 wherein they had to learn to redirect their poking for a new active port
628 location (reversal learning). Shown also is the behavior of these two mice during extinction,
629 wherein the port lights were on (*viz.,* both ports were visually 'active') but no optogenetic

stimulation was available regardless of poking. **(Dii)** A win-loss plot for mouse 127 from session 2-5. **(E)** Quantification of opto-ICSS data indicating that ChR2 mediated stimulation of OT D1 neurons promotes reinforcement and approach behaviors. The first phase of reversal learning resulted in a significant reduction in % pokes for the new active port, which with experience was restored on the last session of the reversal phase.

Supplementary Figure Legends

Supplementary Figure 1. A) Histological verification of pPCX and OT recording sites. **B)** Background firing rate distribution of all pPCX and OT single-units used for analysis. **C)** Summary of learning and performance in the lick/no-lick odor discrimination task for mice contributing single-unit data. Red dashed horizontal line = criterion behavioral performance level.

Supplementary Figure 2. Time course of odor-evoked changes in firing rate separated by response type. Population average auROC values for all responsive neurons in pPCX and OT (same neurons as in Fig. 2), separated by whether the response was excited or suppressed relative to baseline. Population values represent the mean ± SEM.

Supplementary Figure 3. A) Histological verification of optical fiber implants from all mice contributing fiber photometry data. Summary of learning and performance in the lick/no-lick odor discrimination task for D1-Cre **(B)** and D2-Cre mice **(C)** contributing fiber photometry data. Red dashed horizontal line = criterion behavioral performance level.

658 **Methods**

659 *Animals.* Eleven 2-4 months of age male C57bl/6 mice originating from Harlan Laboratories
660 (Indianapolis, IN) were used for single-unit recordings. For fiber photometry, we utilized male
661 bacterial artificial chromosome transgenic mice expressing Cre-recombinase under control of the
662 *drd1a* (D1-Cre; *n* = 7; obtained from the UC Davis Mutant Mouse Regional Resource Center,
663 strain EY262Gsat/Mmucd) or *drd2* gene (D2-Cre; *n* = 7; obtained from the UC Davis Mutant
664 Mouse Regional Resource Center, strain ER44Gsat)(Gong et al., 2003). The offspring of
665 homozygous tdTomato Ai9 reporter mice (Madisen et al., 2012), crossed with D1- or D2-Cre
666 heterozygotes were used to confirm specificity of GCaMP expression. Genotyping was performed
667 following standard protocols using tail tissue DNA. Mice were housed on a 12:12 h light-dark cycle
668 with food and water available *ad libitum*, except when water was restricted for behavioral training
669 (see below). Up to 5 mice were co-housed in a cage before experimentation, but all post-surgical
670 animals were housed individually. All experimental procedures were conducted in accordance
671 with the guidelines of the National Institutes of Health and were approved by the Case Western
672 Reserve University and University of Florida Institutional Animal Care and Use Committees.

673

674 *Methods for multi-site single-unit recordings during lick/no-lick odor discriminations.*

675 Surgical procedures were conducted as described previously (Gadziola et al., 2015; Gadziola &
676 Wesson, 2016). Briefly, mice were anesthetized with Isoflurane (2-4% in oxygen, Abbott
677 Laboratories, Green Oaks, IL), and mounted in a stereotaxic frame with a water-filled heating pad
678 (38°C) beneath to maintain body temperature. An injection of a local anesthetic (0.05% marcaine,
679 0.1 ml s.c.) was administered before exposing the dorsal skull. A craniotomy was made to access
680 the OT and pPCX, each contralateral from another (see **Fig S1A** for distribution). An 8-channel
681 micro-wire electrode array (PFA-insulated tungsten wire, with four electrode wires encased
682 together in a 254 µm diameter polyimide tube (Gadziola et al., 2015)) was implanted within the
683 OT (4.9 mm ventral) and posterior PCX (4.2 mm ventral) (**Fig 1A and S1A**), and cemented in
684 place, along with a headbar for later head fixation. The hemisphere receiving an array into each
685 structure was not held constant across animals but instead varied (**Fig S1A**). Additional
686 craniotomies were drilled over a single neocortex for placement of a stainless steel ground wire.
687 During a three-day recovery period, animals received a daily injection of carprofen (5 mg/kg, s.c.,
688 Pfizer Animal Health, New York, NY) or meloxicam (5mg/kg; Putney, Inc., Portland, ME) and *ad*
689 *libitum* access to food and water. Animals were allowed 5-7 days for post-op recovery before
690 beginning water restriction.

691

692

693 *Olfactory lick/no-lick odor discrimination and reversal learning behavioral task.*

694 Mice were mildly water-restricted for three days prior to behavioral training. Bodyweight was
695 monitored daily and maintained at 85% of their original weight. Mice were trained in cohorts of
696 three to four. All behavioral procedures were performed during the light hours, in a dim room.
697 Head-fixed mice were trained in a lick/no-lick odor discrimination task (**Fig 1C**) across multiple 1
698 hour recording sessions in which the mice obtained a fluid reward for licking a spout positioned in
699 front of their snouts in trials with reinforced odors (Gadziola et al., 2015), adapted from (Verhagen
700 et al., 2007).

701

702 Licking was measured by a pair of infrared photo-beams positioned to cross in front of the lick
703 spout by ~2 mm. Mice were first trained to lick the water spout for reward, with a progressively
704 increasing inter-trial interval (ITI) (3 ± 1 s, Phase 1). In Phase 2, odor presentation began with a
705 10 ± 2 s ITI, and mice were only rewarded for licking during a 2 s period after odor offset (FR1).
706 Licking during the odor was discouraged by moving the lick spout further away from the snout. In
707 Phase 3, trials were randomized between rewarded and unrewarded trials (17 ± 2 sec ITI); for
708 unrewarded odor trials, mice were presented with a “blank” stimulus (mineral oil) and had to learn
709 to withhold licking during these trials. Finally, in Phase 4, trials (17 ± 2 s ITI) were randomized
710 between the rewarded and unrewarded odors. In go trials, mice would receive a reward for licking
711 a spout within 2sec following the offset of the rewarded odor (hit); not licking would be considered
712 a miss. In no-go trials, mice were presented with an unreinforced odor and did not receive a water
713 reward regardless of whether they licked (false alarm) or correctly withheld licking for the total
714 odor duration of the trial (correct reject). Next, mice continued on Phase 5 to learn a novel odor
715 pair. Phase 5 consisted of pseudo-random trials (17 ± 2 s ITI) among which all four odors were
716 separately presented, with the two reinforced odors both resulting in a low-value reward. Finally,
717 in Phase 6, the four odors were presented (17 ± 2 s ITI), with one rewarded odor being assign to
718 the high value saccharine and the other to the low value saccharine. Mice discriminated among
719 the four odors, two of which predicted presentation of reward (either low or high value saccharine),
720 and two unrewarded odors. These sessions include the original training odor set, as well as novel
721 odors presented on a different experimental day (each mouse was shaped on 2 novel sets of four
722 odors on different sessions). No major effects were observed between high versus low value
723 rewarded odor evoked responses nor behavior and therefore herein any odors paired with
724 reinforcers are classified as conditioned rewarded odors, whereas those not paired are termed
725 conditioned unrewarded odors. Throughout all phases, behavioral performance was evaluated in

726 blocks of 20 trials, and mice were required to achieve a performance criterion ≥80% correct for
727 two consecutive blocks in order to advance to the next phase. Neural activity was recorded
728 throughout all training phases, but analysis of odor-evoked activity was restricted to post-training
729 sessions.
730
731 *Stimulus Delivery.*
732 Odors were presented through a custom air-dilution olfactometer with independent stimulus lines
733 up to the point of entry into the odor port. In addition to a blank stimulus (mineral oil), odors
734 included ethyl butyrate, 1,7-octadiene, isopentyl acetate, heptanal, 2-heptanone, (+)-limonene,
735 ethyl propionate, (-)-limonene, methanol, methyl valerate, 2-butanone, 1,4-cineole, butanal,
736 propyl acetate, allylbenzene, allyl bromide, isobutyl propionate, and 2-methylbutyraldehyde
737 (Sigma Aldrich, St. Louis, MO; all >97% purity). These molecularly diverse odors were diluted in
738 their liquid state to 1 Torr (133.32 Pa) in mineral oil and were then further diluted to 10% (vol/vol)
739 by mixing 100 ml odor vaporized N_2 with 900 ml medical grade N_2 (Airgas, Radnor, PA). Thus,
740 stimuli were delivered at a total flow rate of 1 L/min. Not all animals were tested with all odors.
741 The rewarded and unrewarded odor pairs were pseudo-randomly assigned to each cohort prior
742 to training (neurons were not initially screened for odor responsiveness). The experimenter was
743 not blind to odor assignment, but all stimulus presentation was automated. Presentation of
744 rewarded and unrewarded odors were pseudo-randomized within each block, delivered for 2 s
745 duration with a 17 ± 2 s ITI through a Teflon odor-port (9 mm diameter opening) directed towards
746 the animal's snout at a distance of 1 cm. Odor was continuously flowing to the odor-port but was
747 removed by a vacuum before exiting towards the animal. Recordings with a photoionization
748 detector (miniPID, Aurora Scientific, Ontario, Canada) were used to confirm the temporal
749 dynamics of the odor presentation in this design. While the dynamics may vary slightly across
750 odors, they confirm the precision and stability of the odor presentation methods used in this study.
751
752 *Reward Delivery.*
753 Reward fluids were delivered through a custom 3D-printed polylactic acid lick spout, as reported
754 previously (Gadziola and Wesson, 2016). Independent stimulus lines terminated onto 20G
755 blunted needles that passed through one of seven 1-mm holes and extended to the tip of the
756 spout. In the current task, two adjacent holes on the lick spout were used for reward delivery,
757 three were connected to a vacuum line, and the last two unused holes were blocked. Animals
758 were reinforced with a 4μL drop of 2-20mM saccharin (Sigma Aldrich, St. Louis, MO; dissolved in
759 water). Reward volumes were calibrated for the individual reward valves.

In vivo Electrophysiology.

The outputs of the electrode arrays were amplified, digitized at 24.4 kHz, filtered (bandpass 300-5000 Hz), and monitored (Tucker-Davis Technologies, Alachua, FL), along with licking (300 Hz sampling rate), and odor and reward presentation events. One electrode wire was selected to serve as a local reference for each headstage. Our electrode arrays were fixed in place and no attempt was made to record from unique populations of neurons on different sessions. To compensate for the possibility that the same neurons were recorded across multiple days, two different behavioral tasks were employed and statistical comparisons are only made within each task type. Sessions of the same task and odor pair were run for 1-3 consecutive days to achieve adequate behavioral performance and/or capture the dynamics of newly identified neurons. On average, 3.5 ± 1.9 single neurons were identified per mouse per session (range: 1-7 neurons), with an average of 1.4 ± 0.6 neurons recorded per viable electrode wire per mouse per session (range: 1-3 neurons). Numbers were comparable when separated by region (± 0.1 single units / region difference).

Analysis of odor-evoked electrophysiology data.

Single neurons were sorted offline in Spike2 (Cambridge Electronic Design, Cambridge, England), using a combination of template matching and cluster cutting based on principle component analysis. Single neurons were further defined as having <2% of the spikes occurring within a refractory period of 2 ms. Spike times associated with each trial were extracted and exported to MATLAB (Mathworks, Natick, MA) for further analysis. To examine modulations in firing rate within a single trial, spike density functions were calculated by convolving spike trains with a function resembling a postsynaptic potential (Thompson et al., 1996). Mean firing rates across trials were measured in 50 ms bins, along with the 95% confidence interval. Mean baseline firing rate for each neuron was averaged across a 2 s period prior to odor onset.

Animals were typically presented with at least 40 trials of each rewarded and unrewarded odor set per session. To ensure that animals were engaged in the task, only blocks possessing high behavioral performance were analyzed. On some trials, mice may have been licking during odor presentation. Any trials in which the animal licked during the first 1.5s period after odor onset were removed. This ensured that any odor-evoked activity observed during the first several hundred ms was not due to licking-related activity. Of the 11 animals with bilateral implants, 10

792 were confirmed to reside within the OT and 8 within the pPCX. One of the 10 OT-confirmed
793 animals did not contribute data since they did not yield well-isolated neurons. From all mice
794 contributing data, 7 yielded simultaneous OT and pPCX single-units.
795
796 *ROC Analysis.*
797 The area under the receiver operating characteristic (auROC) is a nonparametric measure of the
798 discriminability of two distributions (Green and Swets, 1966). To normalize activity across
799 neurons, we used an auROC method that quantifies stimulus-related changes in firing rate to the
800 baseline activity on a 0-1 scale (for more details see (Cohen et al., 2012)). A value of 0.5 indicates
801 completely overlapping distributions, whereas values of 0 or 1 signal perfect discriminability. We
802 calculated the auROC at each 50-ms time bin over a 4 s period centered on stimulus onset for
803 each neuron. Values greater than 0.5 indicate the probability that firing rates were increased
804 relative to the pre-stimulus background (excitation), whereas values less than 0.5 indicate the
805 probability that firing rates were decreased relative to the pre-stimulus background (inhibition).
806 Similar trial numbers have been used for calculating auROC (Veit and Nieder, 2013; Gadziola et
807 al., 2015, Gadziola & Wesson, 2016). To obtain mean auROC values, the auROC values of
808 individual neurons were averaged at each time bin. In some cases mean auROC values were
809 computed separately for all excitatory and inhibitory neurons.
810

811 *Methods for fiber photometric-based imaging of D1- and D2-type dopamine receptor expressing*
812 *OT neurons during lick/no-lick odor discrimination and reversal learning.*

813 *Virus injection and optical fiber Implantation.* To achieve cell-type specific GCaMP6f (Chen et al.,
814 2013) expression, D1- and D2-Cre mice were injected with AAV5-EF1a-DIO-GCaMP6f-WPRE
815 (5.43^{e13} GC/ml, obtained from the Penn Vector Core in the Gene Therapy Program of the Univ of
816 Pennsylvania). Stereotaxic surgery was performed as described above with exceptions as noted
817 below. 1µl of virus was infused into the OT at a rate of 0.1nl/sec and allowed to diffuse for 10mins
818 before needle was slowly withdrawn over the subsequent 20mins. This injection paradigm was
819 not intended to infect solely OT neurons, but to yield a bolus of infected cells which could be later
820 targeted selectively for imaging by careful localization of the optical fiber. Following, the
821 craniotomy was sealed with wax and the wound margin closed. Animals were allowed 2 weeks
822 for the virus to transduce and then a 400µm core, 0.48NA optical fiber, threaded through metal
823 ferrules were chronically implanted to terminate within the OT. Implants were cemented in place

824 along with a headbar for later head fixation. As with the single-unit recordings, animals were
825 allowed 5-7 days for post-op recovery before beginning water restriction. D1- and D2-Cre mice
826 were tested in mixed cohorts.
827
828 *Imaging.* 465nm (GCaMP excitation wavelength, driven at 210 Hz) and 405nm (UV excitation
829 wavelength, driven at 330Hz; control channel) light emitting diodes were coupled to a 5 port
830 fluorescence mini cube (FMC5, Doric Lenses) using 400µm core, 0.48NA, 2.5mm FCM optical
831 fiber patchcords. Excitation and emission light were directed through a single optical fiber
832 patchcord connected to the animal via a 2.5mm metal ferrule. Emission light was directed through
833 the 5-port mini cube, and subsequently coupled to a pair of femtowatt photoreceivers (model
834 2151, Newport) for monitoring of the GFP and UV fluorescence. Photometry data were digitized
835 and pulse demodulated at 1kHz, along with the timing of behavioral events (licking) and odor and
836 reward delivery using a Tucker Davis Technologies digital processor (TDT). Parameters used for
837 imaging and acquisition of photometry data were held constant across all mice.

838 *Lick/no-lick odor discrimination and reversal learning during photometry.* The methods for
839 operant olfactory behavior employed for fiber photometry were mostly identical to those used
840 for the single-unit recordings (see above) with two exceptions. First, during the fiber photometry
841 imaging, mice were only asked to discriminate between two odors in any given session (one
842 conditioned rewarded and one conditioned unrewarded). Second, mice were shaped in a
843 reversal learning paradigm wherein following reaching successful criterion performance in the
844 original odor discrimination, the contingencies were reversed so that the original rewarded odor
845 no longer signals reinforcement availability (now the 'new unrewarded odor') and the original
846 unrewarded odor now signals reward availability (now the 'new rewarded odor').

847 *Processing and analysis of photometry data.* Off-line, the UV signal was subtracted from that of
848 the GFP, filtered (2nd order, 25Hz low-pass), smoothed, and down sampled to 200Hz using a
849 custom script written in Spike2 (Cambridge Electronic Design, Inc). Photometry recordings were
850 normalized across trials off-line, using the mean signal across 3 sec before odor delivery as a trial
851 specific baseline for the $\Delta F/F$ values. Of the 7 D1-Cre animals with bilateral implants, 1 was
852 confirmed to have poor/weak viral expression and one have a fiber tip residing outside of the OT.
853 Of the 7 D2-Cre mice, 2 were confirmed to have fiber tips residing outside of the OT. Thus, in
854 total, 5 mice per genotype, which had 1) criterion-level behavioral performance, 2) on target OT
855 fiber tips, and 3) quality viral expression contributed data.

856

857 *Methods for optogenetic stimulation of OT D1 expressing neurons and intra-cranial self-*
858 *stimulation.*

859 The surgical methods to allow for expression of ChR2 in OT D1-expressing neurons are similar
860 to those used for GCaMP6f as described above. Two surgical procedures were performed on
861 each mouse. First, mice were intracranially injected with one of two floxed AAV vectors to allow
862 for expression of AAV5.EF1a.DIO.hChR2(H134R).eYFP or mCherry (to yield optogenetic
863 stimulation) or AAV5.EF1a.DIO.eYFP or mCherry (as control). AAVs were obtained from the
864 University of North Carolina viral vector core. Second, mice were intracranially implanted with a
865 unilateral optic fiber (300um, 0.39NA) into their OT which was attached to a ferrule to allow light
866 transmittance into the brain. AAV injections and ferrule implants occurred in the left hemisphere
867 or right hemisphere to prevent biasing results towards effects which may be lateralized. Using a
868 light meter (Thorlabs, Inc., Newton, New Jersey), all fiber optic implants were verified prior to
869 implantation to deliver 6.5-7.5mW[3] of light energy when using the same LED and LED driver as
870 used during Opto-ICSS testing (see below).
871

872 *Opto-ICSS apparatus and light stimulation.* We used a dual nose-poke port apparatus wherein
873 poke into each port is monitored by 880nm infrared photobeams and digitized for later analysis.
874 The floor and three walls of the apparatus were made of black acrylonitrile butadiene styrene
875 (ABS) plastic (30cm tall walls), consisting of a 15 x 15cm square floor and a guillotine style ABS
876 door to allow gentle insertion and removal of the mouse from the testing apparatus. One wall of
877 the apparatus was constructed of clear acrylic to allow visual monitoring of the mouse by an
878 experimenter when needed. The ceiling was 'open' to allow for tethering of the animal to an optical
879 rotary joint (Doric Lenses, Inc., Quebec, Canada) which was suspended above the apparatus.
880 The nose-poke ports were 3D-printed out of polylactic acid plastic and were T-shaped with a 2cm
881 opening which faced into the behavioral apparatus to allow nose-entry and monitoring of infrared
882 beam breaks. Photobeam status (open or closed) was acquired continuously and relayed to a PC
883 for data collection using an Arduino microcontroller board running custom code written in the
884 Arduino open source language (Arduino, https://www.arduino.cc). Immediately next to each port
885 was a 3mm white LED, also controlled by the Arduino, which could signal to the mouse active
886 port status (on = active and optical stimulation available, off = inactive and no available optical
887 stimulation).

888 Optogenetic stimulation (25Hz train, 15ms pulse width, 2 sec duration [for opto-ICSS the 2
889 sec stimulation occurred regardless of the nose-poke duration]) was accomplished by means of
890 a 447.5nm LED (Luxeon Rebel ES, Luxeon Stars, Lethbridge, Alberta) driven by a Thorlabs T-
891 Cube LED driver (Thorlabs) and controlled by the digital output of an Arduino microcontroller. This
892 stimulation paradigm was selected following the results of physiological and behavioral pilot
893 studies. An SMA adapter was adhered atop of the LED using optical epoxy to allow for butt
894 coupling of an SMA terminated multimode fiber to the LED. The fiber used to connect the LED to
895 the optic rotary joint as well as the fiber used to connect the rotary joint to the mouse were both
896 300µm core multimode fibers with a 0.39NA (same as the fiber used for the optical implants),
897 encased in 2mm furcation tubing.
898
899 *Opto-ICSS shaping and testing.* All behavioral procedures were performed during the light hours,
900 in a dim room. At the start of all sessions, the mice were first gently connected to the fiber optic
901 tether. The mice were then placed into the apparatus and the door closed. The stages of shaping
902 and testing in the opto-ICSS task are illustrated in **Figure 4** and occurred on separate daily 60min
903 sessions. In phase 1, both ports were active (both active port LEDs were on) and nose-poke into
904 either port triggered blue light stimulation. After performing ≥ 40 pokes into either or both ports in
905 a given session, for at least two consecutive sessions, mice were then transitioned into phase 2
906 of the task. In phase 2, the port wherein the mouse displayed the greatest number of pokes on
907 subsequent days, was set to be active (port LED on, blue light stimulation available) and the
908 alternative port was inactive (port LED off, blue light stimulation unavailable). Only nose poke into
909 the active port triggered light stimulation. After mice reached criterion performance in phase 2
910 (≥40 pokes, with ≥80% into the active port), they were switched to phase 3 wherein the active and
911 inactive ports were reversed so that the previously inactive port is now the only port which would
912 trigger light stimulation. Phase 3 is thus a test of reversal learning and ensures that the animal's
913 tendency to poke is indeed motivated by light-mediated ChR2 stimulation. Those mice which
914 reached criterion performance on phase 3 (see above), were advanced onto phase 4. In all of the
915 previous phases stimulation was available on an FR1 (fixed ratio of 1) schedule. In phase 4, both
916 ports were rendered inactive (both port LEDs were off, blue light off) in a test of extinction.
917 Transitions between phases occurred on subsequent daily testing sessions. Mice which did not
918 reach criterion performance on a given phase by the end of the 6th session of that phase were
919 eliminated from further testing.

920

921 *Histology*

922 Following the end of experiments, mice were overdosed with Fatal-plus (0.01mL/g; Vortech
923 Pharmaceutical, Dearborn, MI) and perfused with 10mL of cold saline followed by 15mL of cold
924 10% phosphate buffered formalin. Brains were stored in 10% formalin/30% sucrose (4ºC) prior to
925 sectioning at 40µm thickness on a Leica sliding microtome. Tissue was later mounted on slides
926 using Fluoromount-G containing DAPI (for fluorescence analysis; 4',6-diamidino-2-phenylindole;
927 Invitrogen, Carlsbad, CA) or stained with 1% cresyl-violet (for tissue contributing single-unit data).
928 Microscopic examination of tissue was conducted on a Nikon Ti2e inverted fluorescent
929 microscope equipped with 5MP color and 15MP monochrome cameras. Histological definition of
930 brain regions was aided by use of a brain atlas (Paxinos and Franklin, 2000). Quantification of
931 fluorophore colocalization (*i.e.,* as in the case of D1-Cre;Ai9 and D2-Cre;Ai9 GCaMP6f injections)
932 was performed using semi-automated methods in NIS Elements (Nikon). Briefly, background
933 fluorescence was decreased to enhance contrast, cells were detected based upon their
934 fluorescence intensity (via a threshold) and their size, and detected objects next post-processed
935 based upon their area to eliminate fluorescent objects which were not cell bodies (*e.g.,* brightly
936 labeled fibers). Counts of tdTomato (Ai9), GFP (GCaMP), and colocalized OT cells (including all
937 OT cell layers) were next automatically exported following manual setting of OT boundaries.

938

939 *Overall statistical methods*

940 All performed tests were two-sided and met assumptions of normality (Kolmogorov-Smirnov test).
941 Sample sizes are consistent with numbers reported in the field and no statistical method was used
942 to predetermine these. Statistical analyses were performed in SPSS 22.0 (SPSS Inc., Chicago,
943 IL) or MATLAB. All data are reported as mean ± SD unless otherwise noted. Specific details
944 regarding some analytical methods (*e.g.,* ROC) can be found in above sections.
945

Figure 1

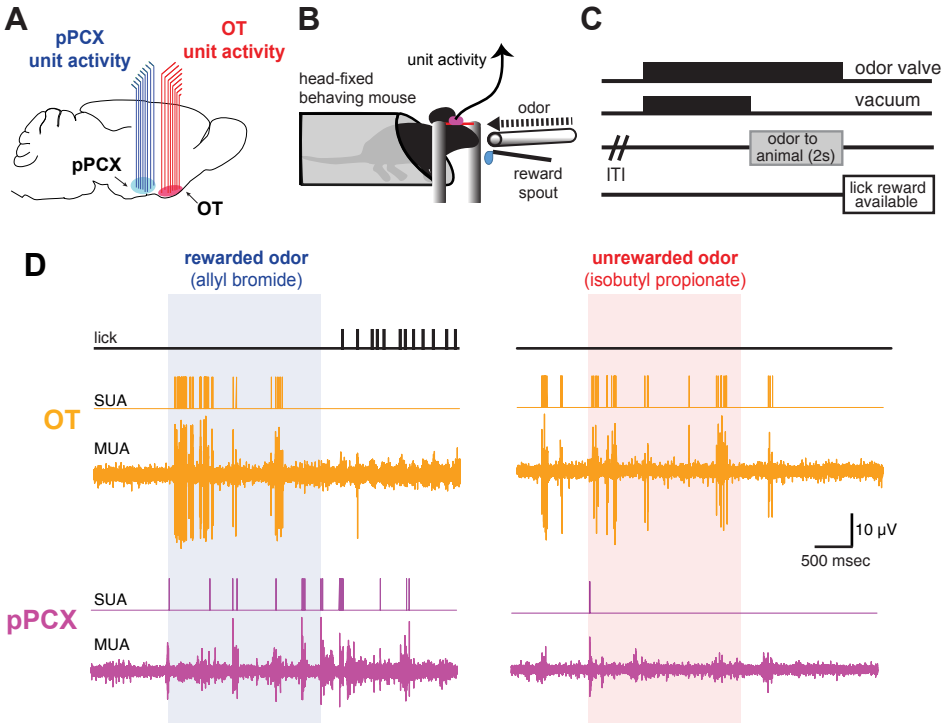
A
pPCX
unit activity
OT
unit activity
pPCX
OT
B
unit activity
head-fixed
behaving mouse
odor
reward
spout
C
odor valve
vacuum
odor to
animal (2s)
ITI
lick reward
available
D
rewarded odor
(allyl bromide)
unrewarded odor
(isobutyl propionate)
lick
OT
SUA
MUA
10 μV
500 msec
pPCX
SUA
MUA

Figure 2

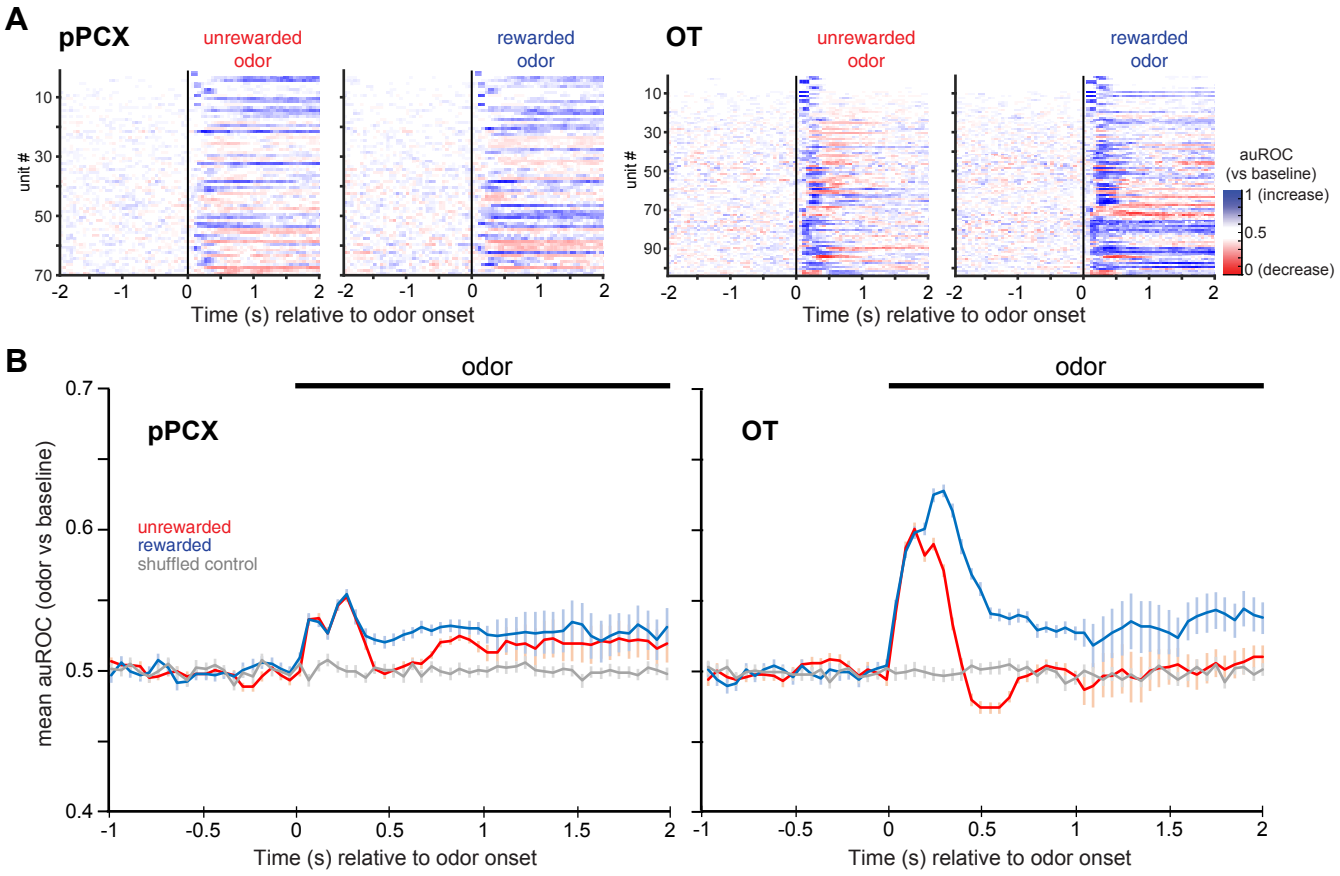
A
pPCX
unrewarded odor
rewarded odor
OT
unrewarded odor
rewarded odor
unit #
Time (s) relative to odor onset
auROC (vs baseline)
1 (increase)
0.5
0 (decrease)
B
odor
pPCX
OT
unrewarded
rewarded
shuffled control
mean auROC (odor vs baseline)
Time (s) relative to odor onset

Figure 3

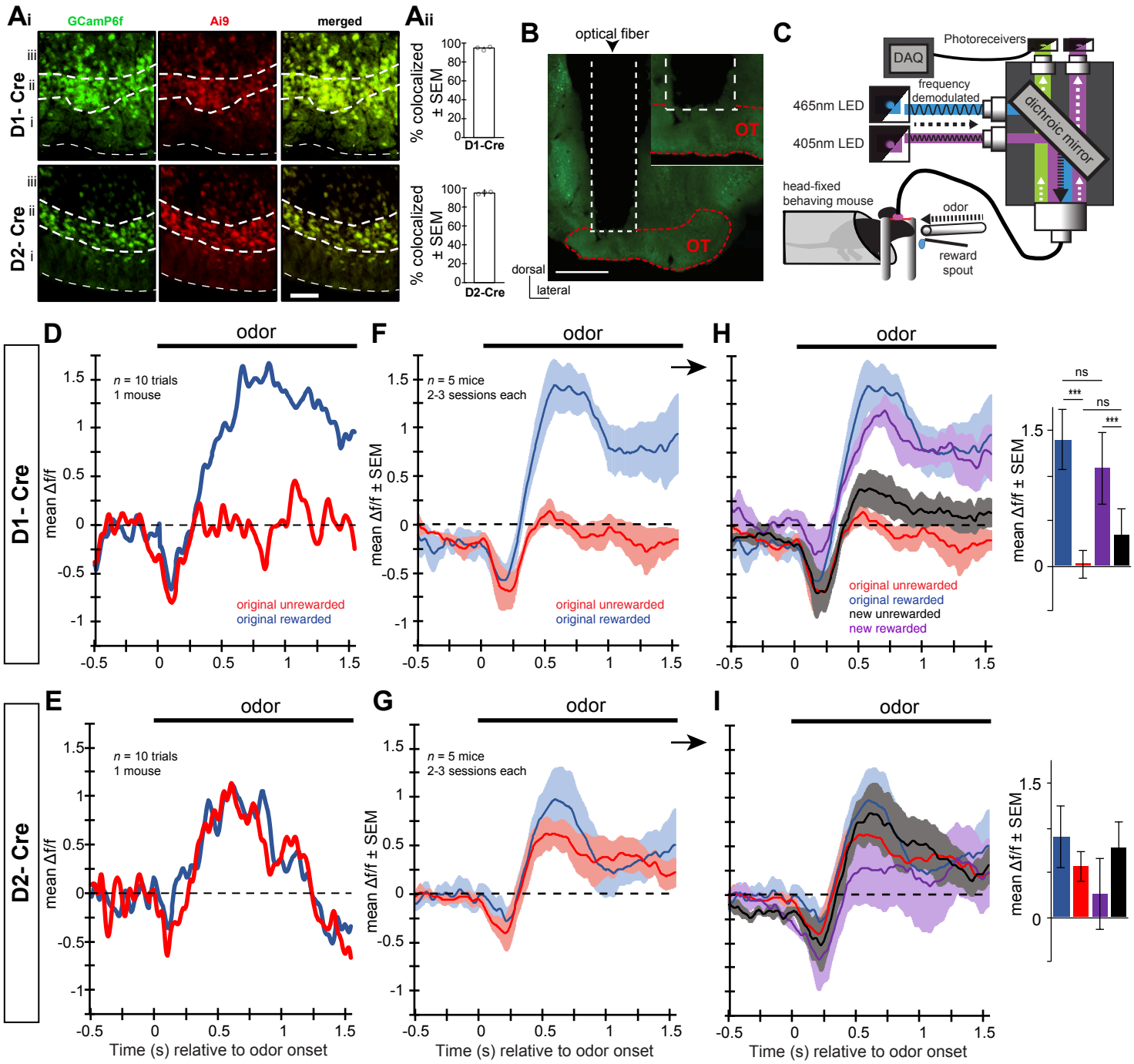
Ai
GCamP6f
Ai9
merged
D1- Cre
D2- Cre
Aii
% colocalized ± SEM
D1-Cre
D2-Cre
B
optical fiber
OT
dorsal
lateral
C
DAQ
Photoreceivers
frequency demodulated
465nm LED
405nm LED
dichroic mirror
head-fixed behaving mouse
odor
reward spout
D
E
F
G
H
I
odor
n = 10 trials
1 mouse
n = 5 mice
2-3 sessions each
mean Δf/f
mean Δf/f ± SEM
original unrewarded
original rewarded
new unrewarded
new rewarded
ns
***
Time (s) relative to odor onset

Figure 4

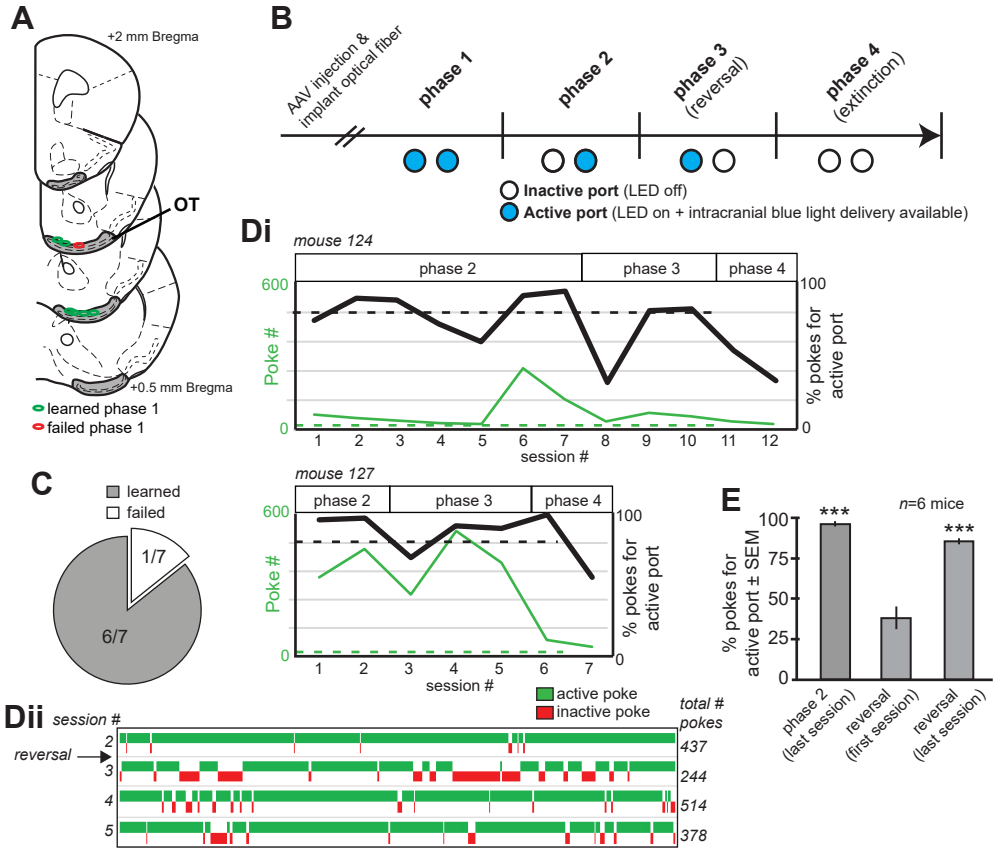
A
+2 mm Bregma
OT
+0.5 mm Bregma
learned phase 1
failed phase 1
B
AAV injection & implant optical fiber
phase 1
phase 2
phase 3 (reversal)
phase 4 (extinction)
Inactive port (LED off)
Active port (LED on + intracranial blue light delivery available)
Di
mouse 124
phase 2
phase 3
phase 4
Poke #
% pokes for active port
session #
mouse 127
C
learned
failed
1/7
6/7
E
n=6 mice
% pokes for active port ± SEM
phase 2 (last session)
reversal (first session)
reversal (last session)
Dii
session #
reversal
active poke
inactive poke
total # pokes
437
244
514
378

Figure S1

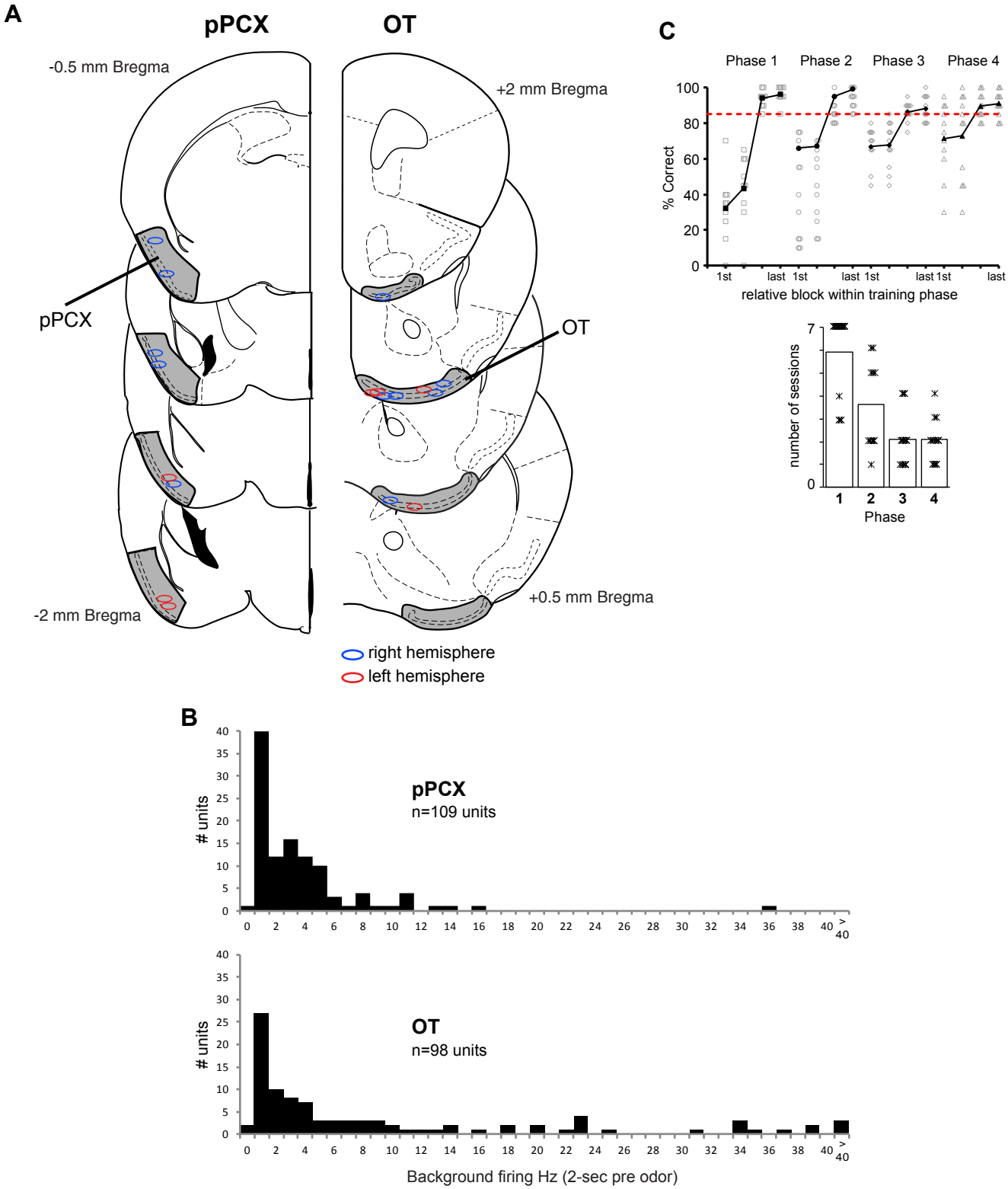
A
pPCX
OT
-0.5 mm Bregma
+2 mm Bregma
pPCX
OT
-2 mm Bregma
+0.5 mm Bregma
right hemisphere
left hemisphere
C
Phase 1
Phase 2
Phase 3
Phase 4
% Correct
relative block within training phase
number of sessions
Phase
B
pPCX
n=109 units
OT
n=98 units
# units
Background firing Hz (2-sec pre odor)

Figure S2

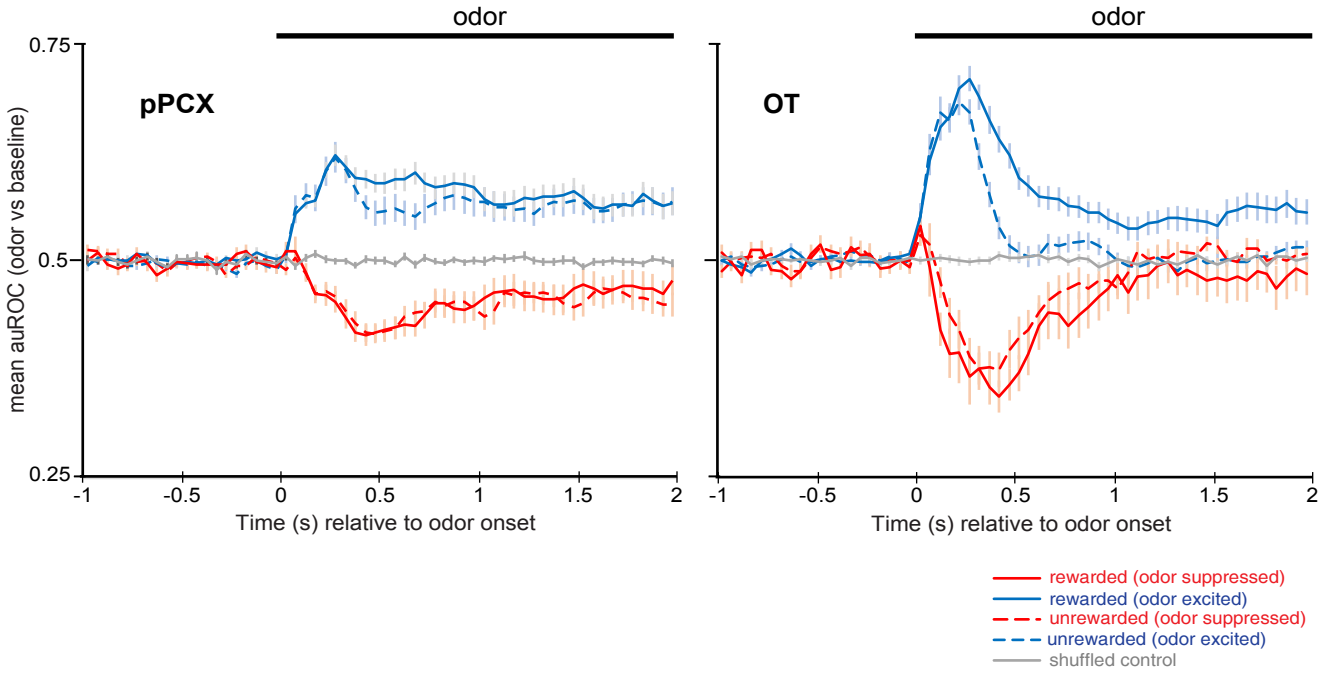
odor
odor
pPCX
OT
mean auROC (odor vs baseline)
0.75
0.5
0.25
-1
-0.5
0
0.5
1
1.5
2
Time (s) relative to odor onset
Time (s) relative to odor onset
rewarded (odor suppressed)
rewarded (odor excited)
unrewarded (odor suppressed)
unrewarded (odor excited)
shuffled control

Figure S3

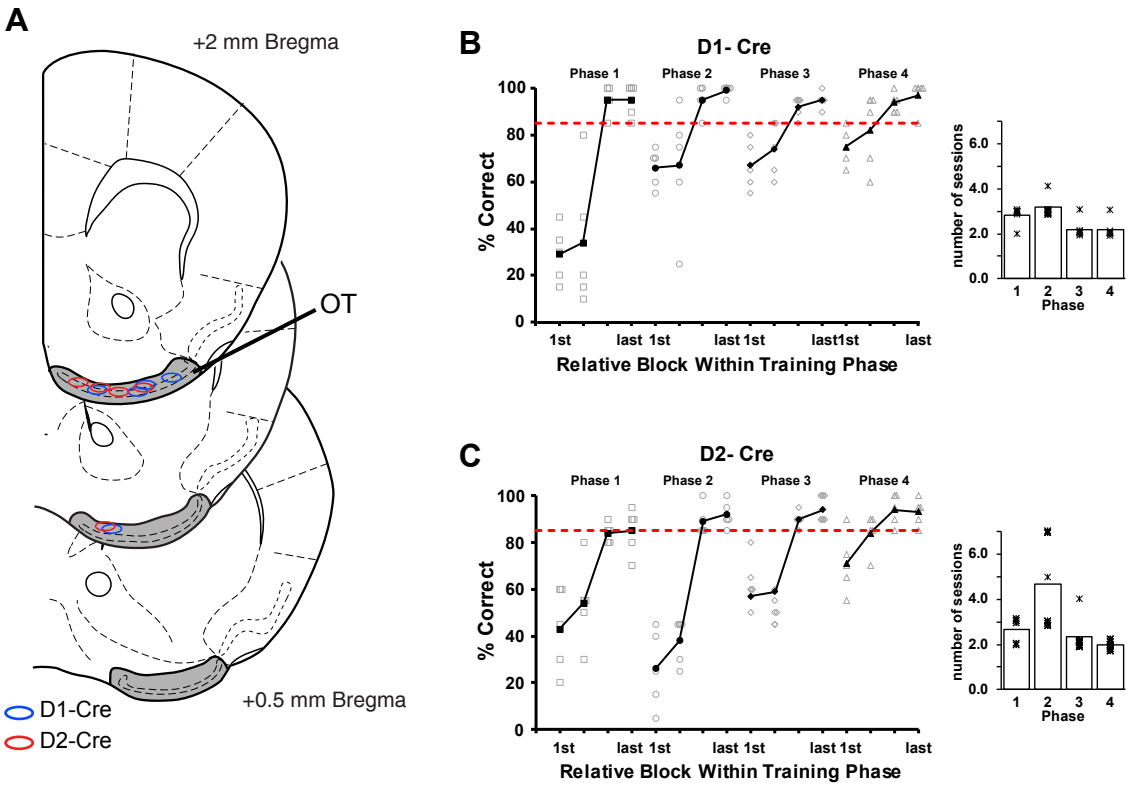
A
+2 mm Bregma
OT
+0.5 mm Bregma
D1-Cre
D2-Cre
B
D1- Cre
Phase 1
Phase 2
Phase 3
Phase 4
% Correct
Relative Block Within Training Phase
1st
last
number of sessions
Phase
C
D2- Cre